

Liquid Nanodroplets Spreading on Chemically Patterned Surfaces

Gary S. Grest, David R. Heine[†], and Edmund B. Webb III*

Sandia National Laboratories, Albuquerque NM 87185

[†]*Present address - Corning Incorporated, Painted Post, New York 14870*

**Author to whom correspondence should be addressed; email: ebwebb@sandia.gov*

(Dated: July 17, 2018)

Abstract

Controlling the spatial distribution of liquid droplets on surfaces via surface energy patterning can be used to control material delivery to specified regions via selective liquid/solid wetting. While studies of the equilibrium shape of liquid droplets on heterogeneous substrates exist, much less is known about the corresponding wetting kinetics. We make significant progress towards elucidating details of this topic by studying, via large-scale atomistic simulations, liquid nanodroplets spreading on chemically patterned surfaces. A model is presented for lines of polymer liquid (droplets) on substrates consisting of alternating strips of wetting (equilibrium contact angle $\theta_0 \simeq 0^\circ$) and non-wetting ($\theta_0 \simeq 90^\circ$) material. Droplet spreading is compared for different wavelength λ of the pattern and strength of surface interaction on the wetting strips. For small λ , droplets partially spread on both the wetting and non-wetting regions of the substrate to attain a finite contact angle less than 90° . In this case, the extent of spreading depends on the interaction strength in the wetting regions. A transition is observed such that, for large λ , the droplet spreads only on the wetting region of the substrate by pulling material from non-wetting regions. In most cases, a precursor film spreads on the wetting portion of the substrate at a rate strongly dependent upon interaction strength.

I. INTRODUCTION

The spreading of a liquid droplet on a surface proceeds as the droplet balances the interfacial tensions between the solid, liquid, and vapor phases. On a homogenous substrate, completely wetting droplets (i.e. where the equilibrium contact angle $\theta_0 = 0^\circ$) often form a monolayer film or precursor foot on the surface that spreads ahead of the main droplet. This has been observed in experiments [1, 2, 3, 4] as well as simulation [5, 6, 7, 8, 9]. This foot grows diffusively with an effective diffusion constant D_{eff} that depends on the square root of the initial radius R_o of the droplet [10]. While much has been revealed about the kinetics of droplets spreading on homogenous surfaces, spreading on chemically patterned surfaces is much less understood. In particular the influence of the pattern feature size on the spreading rate of both the precursor foot and main droplet is unknown.

With the advent of modern lithography techniques, it is now possible to chemically pattern a substrate with lyophobic and lyophilic surface domains on the nano to micron scale [11]. These chemically structured surfaces can be useful in controlling the wetting of liquid droplets. Depending on the size of the pattern and the contact angle in the two domains, wetting transitions can occur in which the liquid droplet can change its shape or morphology [12, 13]. The equilibrium shapes of liquid droplets on a variety of chemically patterned surfaces has been studied both experimentally and theoretically [14, 15, 16, 17, 18, 19, 20]. Introduction of a lyophobic grid can be used to confine liquid droplets and has been shown to improve the quality of ink jet printing [21]. In most of these studies, the liquid droplet is confined by the pattern of lyophilic and lyophobic domains and does not spread.

An alternate situation occurs if one places a long liquid line transverse to a chemically striped surface of alternating lyophilic and lyophobic domains. This is the situation we study here for the case of liquid polymer droplets of varying chain length. For small λ , the main droplet partially wets both regions of the surface equivalently and does not spread even in the wetting region. For sufficiently large λ the main droplet spreads on the wetting region of the substrate by pulling material from non-wetting regions. In most cases, a precursor film spreads on the wetting portion of the substrate at a rate strongly dependent upon interaction strength even when the main droplet does not spread.

II. COMPUTATIONAL PROCEDURE

Here we present extensive molecular dynamics (MD) simulations of the spreading of short chain polymer droplets spreading on a chemically patterned surface. The polymers are modeled by a coarse grained bead spring model in which each polymer contains N beads per chain with $N = 10$ and 100 . As the entanglement length $N_e \simeq 72$ for this model [22], the chains are unentangled. The polymer is represented by spherical beads of mass m attached by springs, which interact with a truncated Lennard-Jones (LJ) potential,

$$U_{LJ}(r) = \begin{cases} 4\varepsilon \left[\left(\frac{\sigma}{r}\right)^{12} - \left(\frac{\sigma}{r}\right)^6 \right] & r \leq r_c \\ 0 & r > r_c \end{cases} \quad (1)$$

where ε and σ are the LJ units of energy and length and the cutoff $r_c = 2.5\sigma$. The monomer-monomer interaction ε is used as the reference and all monomers have the same diameter σ . For bonded monomers, we apply an additional potential where each bond is described by the FENE potential [23] with $k = 30 \varepsilon / \sigma^2$ and $R_0 = 1.5 \sigma$. The substrate is modeled as a flat surface since it was found previously [8] that with the proper choice of thermostat, simulations using a flat surface exhibit the same behavior as a realistic atomic substrate with greater computational efficiency.

The interactions between the surface and the monomers in the droplet at a distance z from the surface are modeled using an integrated LJ potential,

$$U_{LJ}^{wall}(z) = \begin{cases} \frac{2\pi\varepsilon_w}{3} \left[\frac{2}{15} \left(\frac{\sigma}{z}\right)^9 - \left(\frac{\sigma}{z}\right)^3 \right] & z \leq z_c \\ 0 & z > z_c \end{cases} \quad (2)$$

where ε_w is the monomer-surface interaction strength and $z_c = 2.2\sigma$. Extending the range of this surface interaction to infinity shifts the wetting transition to a lower energy; however, the qualitative spreading behavior is identical to the $z_c = 2.2\sigma$ case [10]. For $z_c = 2.2\sigma$, the critical wetting strength (i.e. $\theta_0 \rightarrow 0^\circ$) is $\varepsilon_w^c \simeq 1.75\varepsilon$ for $N = 10$ and $\varepsilon_w^c \simeq 2.25\varepsilon$ for $N = 100$ [9]. The system is periodic in the y direction with length L_y and open in the other two directions. The chemical pattern consists of infinite strips of wetting and non-wetting regions of equal width $\lambda/2$ as shown in Figs. 1-2 and Fig. 4. In the present simulations the monomer/wall interaction ε_w depends on the position of each monomer in the y direction. For the non-wetting region, ε_w was chosen so that $\theta_0 \simeq 90^\circ$, which for $N = 10$ is $\varepsilon_w = 0.9\varepsilon$ and for $N = 100$ is $\varepsilon_w = 1.0\varepsilon$ [9]. In the wetting region, two cases were studied for $N = 10$:

$\varepsilon_w = 2.0\varepsilon$ and $\varepsilon_w = 3.0\varepsilon$, corresponding to weak and strong wetting, respectively. For $N = 100$, $\varepsilon_w = 2.5\varepsilon$, which is in the weak wetting regime. All of the droplets presented here are modeled as hemicylinders as described previously [9] with initial droplet radii $R_0 \cong 50\sigma$. The effect of varying R_0 for homogeneous droplets has been studied previously [10].

To provide a realistic representation of the transfer of energy in the polymer droplet, a Langevin thermostat is applied only near the surface,

$$m_i \frac{d^2 \mathbf{r}_i}{dt^2} = -\Delta U_i - m_i \gamma_L \frac{d\mathbf{r}_i}{dt} + \mathbf{W}_i(t), \quad (3)$$

where m_i is the mass of monomer i , \mathbf{r}_i is the position of monomer i , γ_L is the friction coupling term for the Langevin thermostat, $-\Delta U_i$ is the force acting on monomer i due to the potentials defined above, and $\mathbf{W}_i(t)$ is a Gaussian white noise term. We use a Langevin coupling term with a damping rate that decreases exponentially away from the substrate [24], $\gamma_L(z) = \gamma_L^s \exp(\sigma - z)$. Here $\gamma_L^s = 3.0\tau^{-1}$ and z is the distance from the substrate. The effect of varying γ_L^s for homogeneous surfaces has been discussed in ref. [8]. By including only a coupling of monomers near the surface to the thermostat, we avoid the unphysical effect of screening the hydrodynamic interactions in the droplet. We also damp monomers near the surface stronger than those in the bulk, which is a more physically reasonable description of dissipation mechanisms due to the surface interaction.

In the simulations L_y varied from 60σ to 200σ , depending on the periodicity of the pattern λ . For $\lambda \leq 60\sigma$, $L_y = 60\sigma$ while for $\lambda \geq 100\sigma$, $L_y = \lambda$. Results for a homogenous wetting substrate, labeled $\lambda = \infty$ are for $L_y = 60\sigma$. The total size of the droplets varied from $N \cong 200\,000$ to $680\,000$ monomers depending on the value of L_y . The vapor pressure is low so that spreading does not occur via vaporization and condensation. However for small λ , particularly for $N = 10$, a few chains separate from the precursor foot and randomly diffuse on to the non-wetting region of the substrate and sometimes evaporate from the substrate. These chains are subsequently removed from the simulation once they move away from the surface a distance several times R_0 .

The equations of motion are integrated using a velocity-Verlet algorithm with a time step of $\Delta t = 0.01 \tau$ where $\tau = \sigma \left(\frac{m}{\varepsilon}\right)^{1/2}$. The simulations are performed at a temperature $T = \varepsilon/k_B$ using the LAMMPS code [25], modified to include the chemically patterned surface. The instantaneous contact radius for the main droplet $r_b(t)$ and the radius of the precursor foot $r_f(t)$ are determined every 400τ according to the procedure described previously [9].

Briefly, the system is divided into layers of thickness 1.5σ parallel to the interface. Data presented for foot kinetics are obtained from the layer closest to the surface (layer 1) and data for bulk kinetics are obtained from layer 4, which is far enough above the substrate to provide an accurate description of bulk droplet behavior.

III. RESULTS

Time sequences for $N = 10$ and $N = 100$ are shown in Fig. 1 for $\lambda = 200\sigma$. For the main droplet to spread (bulk spreading), the gain in interface energy must exceed the cost of increasing the surface area of the droplet. This balance depends on λ , N , and ε_w . For $N = 10$, bulk spreading occurs on the lyophilic strip as material is transferred from the non-wetting to the wetting region. As such, the cross-section of material in the non-wetting region shrinks while maintaining a hemi-cylinder shape with contact angle near 90° . At later time in the simulation, material is completely removed from non-wetting regions. Given periodicity in the y direction, this demonstrates a case where an initial line of liquid (in y) transforms into a series of parallel liquid strips (in x) with separation distance in y equal to $\lambda/2$. For $N = 100$, evidence of N dependence is observed in that bulk spreading does not occur on the wetting region. A precursor film or foot is observed to spread ahead of the main droplet on the lyophilic strip in both systems. Thus, even when the main droplet does not spread, a precursor foot may spread on the wetting region of the substrate. For all cases where a foot was observed to spread, the contact radius follows $r_f^2(t) = 2D_{\text{eff}}t$ where D_{eff} is the effective diffusion coefficient. For $N = 10$ and $\lambda = 200\sigma$ (Fig. 1), the effective diffusion constant D_{eff} of the precursor foot is essentially equal to that for the pure wetting case $\lambda = \infty$. Spreading of the precursor foot for $N = 100$ causes depletion of material on the wetting region. Furthermore, bulk material is unable to move quickly enough from the non-wetting region to the wetting region, resulting in the formation of a saddle shape at the center of the droplet. At late times, the precursor film spreads by polymer moving perpendicularly from the non-wetting to the wetting region, then continuing along the wetting region. In this case D_{eff} is 40% of that for $\lambda = \infty$. Although we do not access such time scales in our simulations, we expect that material will completely wick away from the non-wetting region as the precursor film continues to spread.

Figure 2 presents snapshots of $N = 10$ droplets at late time for varying λ . The snapshots

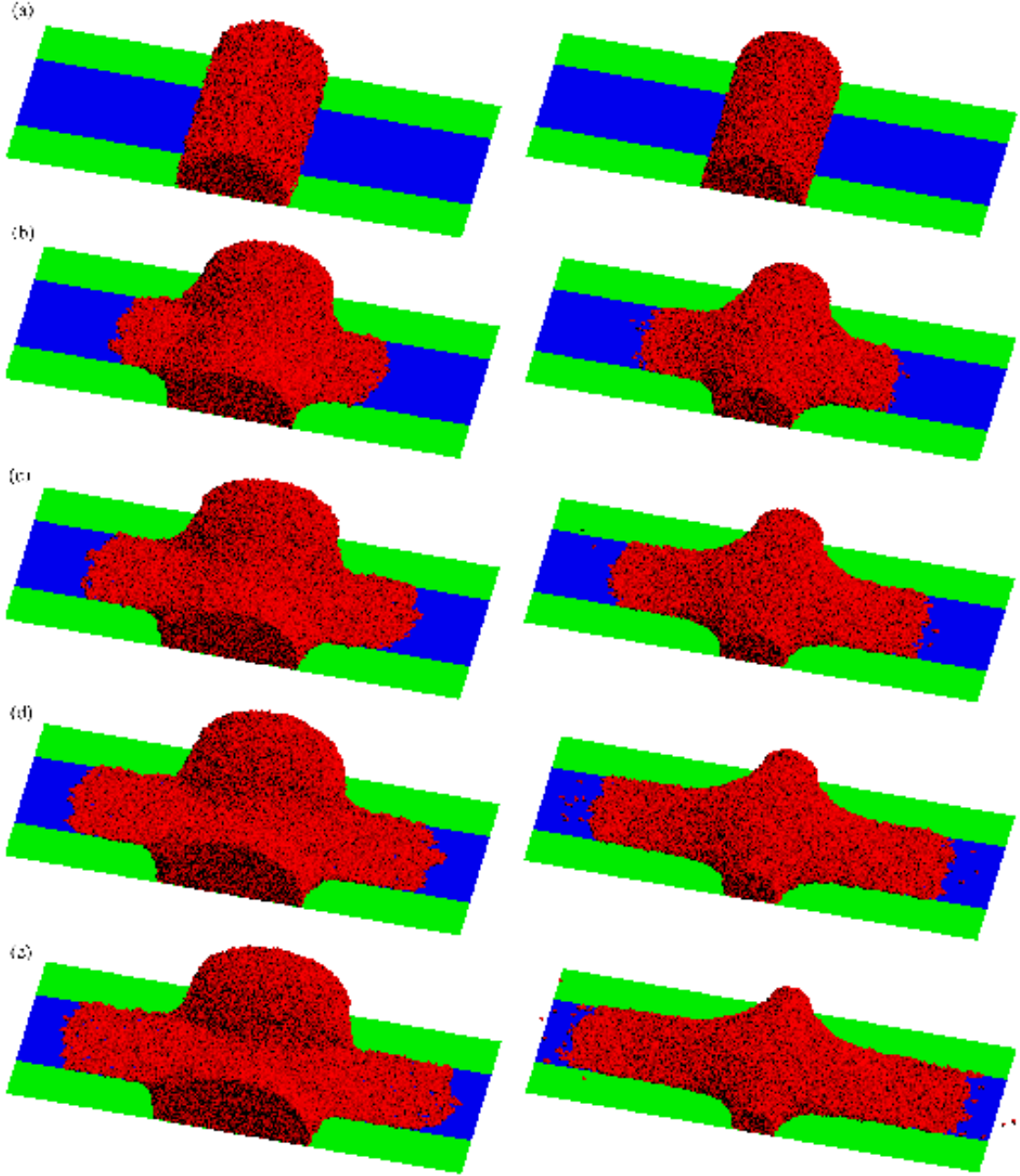


FIG. 1: (color) Sequence of simulation snapshots for the $N = 100$ (left) and $N = 10$ (right) droplets for $\lambda = 200\sigma$ for (a) $t = 0$, (b) $t = 12,000$, (c) $t = 24,000$, (d) $t = 36,000$, (e) $t = 48,000\tau$. For $N = 100$, in non-wetting regions $\varepsilon_w = 1.0\varepsilon$ (green), while in wetting regions $\varepsilon_w = 2.5\varepsilon$ (blue). For $N = 10$, the corresponding values are $\varepsilon_w = 0.9\varepsilon$ (green) and $\varepsilon_w = 2.0\varepsilon$ (blue). The substrate is 425σ long and width $L_y = \lambda$.

are shown at different times chosen so that the size of the precursor foot, when the foot spreads ahead of the droplet, is approximately the same size in each snapshot. In the weak wetting case (Fig. 2, left panels), the main droplet increases in size only slightly before saturating for $\lambda \leq 100\sigma$ as shown in Fig. 3. For $\lambda = 30\sigma$, the bulk droplet saturates at a radius $r_b \cong 60\sigma$ in both the wetting and non-wetting regimes. As λ increases, the radius of the droplet in the non-wetting region decreases while the radius of the droplet in the wetting regime increases slightly. For $\lambda \geq 150\sigma$, the main droplet spreads. Similar to the behavior seen in Fig. 1 for $\lambda = 200\sigma$, the $\lambda = 150\sigma$ system in Fig. 2d (left) shows that the cross-section of material in the non-wetting region shrinks as the bulk droplet in the wetting region continually spreads. For $\lambda = 150\sigma$, the radius of the droplet in the wetting regime continues to grow at late time as shown in Fig. 3. Between $\lambda = 100\sigma$ and 150σ the gain in surface energy exceeds the cost of increasing the surface area and material is able to be drawn continually from the non-wetting region to the wetting region. Figure 2 (right) presents $N = 10$ results for the strong wetting case. Compared to the weak wetting case where spreading of a precursor foot was nearly absent for $\lambda = 30\sigma$, Fig. 2a (right) clearly shows precursor spreading. A separate simulation of the strong wetting system with $\lambda = 20\sigma$ showed a precursor foot spreads even for this very small feature size. It is also apparent, especially for smaller λ , that the stronger interaction in the wetting region causes more spreading in the non-wetting region. The $\lambda = 150\sigma$ case for strong wetting is not shown in Fig. 2; however, similar to the weak wetting case, the minimum width on which the bulk droplet spreads is between $\lambda = 100$ and 150σ . This indicates that the bulk wetting transition is related more to λ than to the strength of interaction in the wetting region ϵ_w . For reference, $\lambda = \infty$ is shown for the strong wetting case in Fig. 2d (right).

$N = 100$ results for different λ are shown in Fig. 4. At $\lambda = 60\sigma$, which is about 4 times the average end-to-end distance of the chain in the melt, the droplet spreads at early time to a radius $r_b \cong 80\sigma$ before reaching its equilibrium size. This final size is comparable to what is observed for a homogenous surface with a mean surface interaction strength, $\bar{\epsilon}_w \simeq 1.75\epsilon$. For $\lambda = 100\sigma$ (Fig. 4b) and 200σ (Fig. 1), the bulk radii in the wetting region saturate at lower values, $r_b \approx 70\sigma$. These data demonstrate that, for sufficiently small feature size, a mean interaction description is fairly accurate but becomes less so for increasing feature size. For $\lambda \geq 60\sigma$ a precursor foot spreads ahead of the droplet while for $\lambda \leq 30\sigma$ no foot is observed. The width λ above which the main droplet spreads on the lyophilic strip is larger

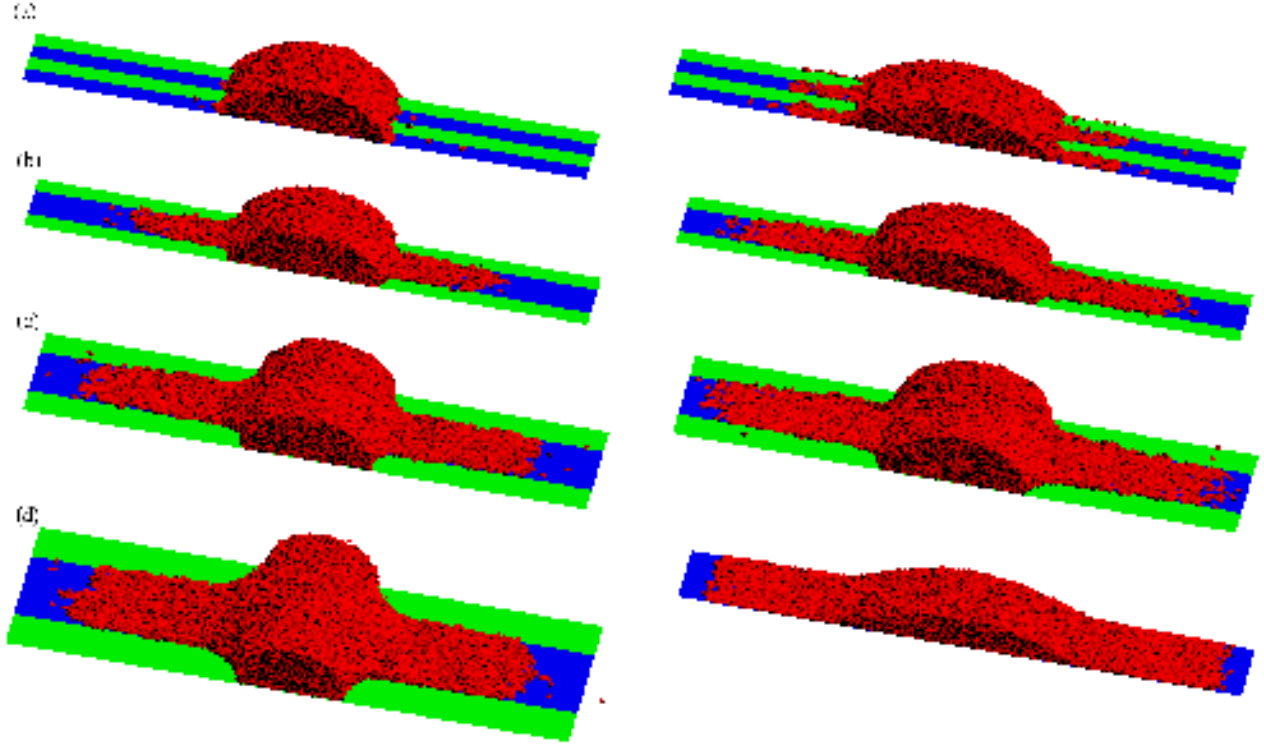


FIG. 2: (color) Simulation snapshots for $N = 10$ polymer droplets; in all cases shown, the interaction strength of the wall in the non-wetting regions (green) is $\varepsilon_w = 0.9\varepsilon$. For panels on the left, the interaction strength in the wetting regions (blue) is $\varepsilon_w = 2.0\varepsilon$ while on the right $\varepsilon_w = 3.0\varepsilon$. In panels (a) - (c), snapshots are presented at $t = 80,000\tau$ (left) and $t = 30,000\tau$ (right) while in panel (d) $t = 48,000\tau$ (left) and $t = 15,000\tau$ (right). Pattern lengths are (a) $\lambda = 30\sigma$, (b) $\lambda = 60\sigma$, (c) $\lambda = 100\sigma$, and (d) $\lambda = 150\sigma$ (left) or (d) $\lambda = \infty$ (right). The substrate is 450σ long in each snapshot, while the width $L_y = \lambda$ except for $\lambda = 30\sigma$ and $\lambda = \infty$, where $L_y = 60\sigma$.

than we can access with present computational resources. For comparison purposes, Fig. 4c presents data for $\lambda = \infty$ and it is obvious that the main droplet spreads for this limit of pattern size.

The contact radius of the precursor foot increases as $r_f^2(t) = 2D_{\text{eff}}t$ for all cases studied. The effective diffusion constant D_{eff} normalized by its value for the homogeneous wetting case is shown in Fig. 5. A result observed in all cases is that D_{eff} increases monotonically with λ . Of note is an apparent cross-over in observed behavior with decreasing λ for the $N = 10$ strong and weak wetting systems. Data imply that, at large pattern width, foot

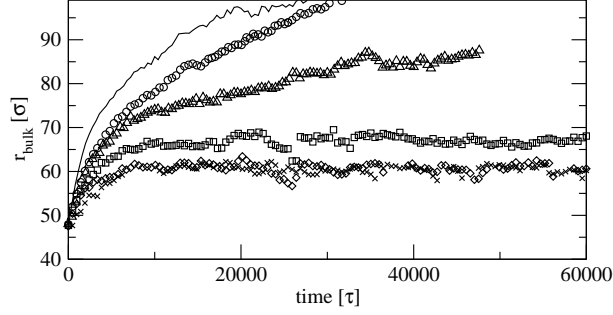


FIG. 3: Radii of the bulk droplets for $N = 10$ in the center of the wetting regions for the weak wetting case $\varepsilon_w = 0.9$ and 2.0ε for $\lambda = 30\sigma$ (crosses), $\lambda = 60\sigma$ (diamonds), $\lambda = 100\sigma$ (squares), $\lambda = 150\sigma$ (triangles), $\lambda = 200\sigma$ (circles), and $\lambda = \infty$ (solid).

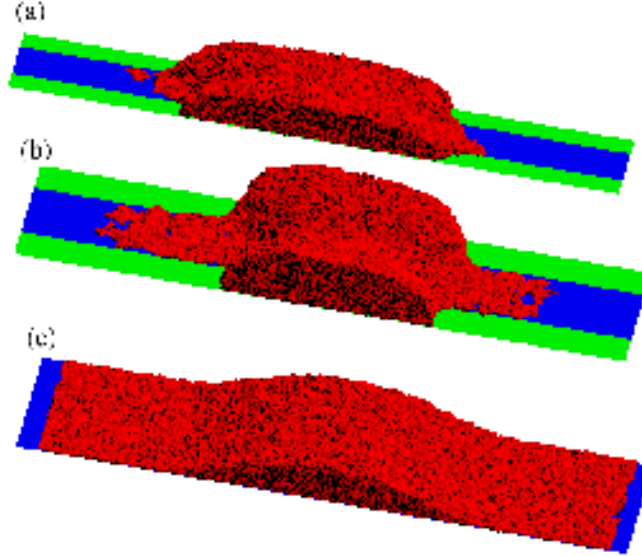


FIG. 4: (color) Simulation snapshots for $N = 100$ polymer droplets with $\varepsilon_w = 1.0\varepsilon$ (green) and $\varepsilon_w = 2.5\varepsilon$ (blue) for (a) $\lambda = 60\sigma$ at $t = 96,000\tau$, (b) $\lambda = 100\sigma$ at $t = 96,000\tau$, and (c) $\lambda = \infty$ at $t = 32,000\tau$. The substrate is 425σ long in each snapshot, while the width $L_y = \lambda$ except for $\lambda = \infty$, where $L_y = 60\sigma$.

transport for the stronger wetting system is more affected by the presence of a lyophobic region than it is for the weaker wetting system. We hypothesize that this results from the very aggressive rate of transport for the foot on the stronger wetting substrate. The system must supply material to the foot from the bulk of the droplet. The rate of foot advancement

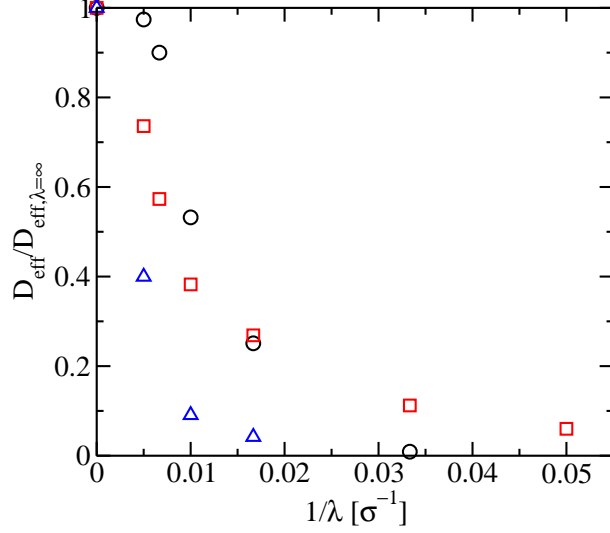


FIG. 5: Normalized effective diffusion coefficient for the precursor foot as a function of the surface pattern wavelength λ for $N = 10$, $\varepsilon_w = 0.9\varepsilon$ and 2.0ε (circles), $N = 10$, $\varepsilon_w = 0.9\varepsilon$ and 3.0ε (squares), $N = 100$, $\varepsilon_w = 1.0\varepsilon$ and 2.5ε (triangles). For $R_0 = 50\sigma$, the values for $D_{\text{eff},\lambda=\infty} = 0.17$ (circles), 0.75 (squares), and $0.33\sigma^2/\tau$ (triangles).

is large enough in the strong wetting case that it becomes limited by transport of material from the non-wetting region to the wetting region, and on to the foot. This is only true for large pattern width $\lambda > 60\sigma$ where the foot is comprised of a more significant amount of polymer material. Note that foot transport along the lyophilic strip is observed for $\lambda < 30\sigma$ in the strong wetting system whereas it is not for the weaker interaction. In our previous work [10] studying wetting on homogeneous substrates, we found that D_{eff} increased with the size of the initial droplet as $R_0^{1/2}$. While we have not varied the size of the initial droplet in this study, we expect a similar dependence of D_{eff} on the initial size of the droplet.

IV. CONCLUSION

Chemically patterning a surface offers a unique opportunity to control the spreading of liquid nanodroplets. Here we have presented simulation results which demonstrate the interplay between the pattern width λ , the length of the polymer chain N , and the interaction strength of the lyophilic strips in determining spreading behavior. We find that there exists a minimum λ , which is a function of N , below which spreading of the main droplet does

not occur. For $N = 10$, a bulk spreading transition with increasing λ was observed, while for $N = 100$, the transition occurs for λ larger than is presently accessible. In a number of cases, a precursor foot is observed to spread even when the main droplet does not spread. The observed effective diffusion constant of this precursor foot decreases monotonically with λ . Future work will reveal the dependence of observed kinetics on the initial size of the droplet and specify the relation between N , λ , and wetting transition.

Acknowledgments

Sandia is a multiprogram laboratory operated by Sandia Corporation, a Lockheed Martin Company, for the United States Department of Energy's National Nuclear Security Administration under contract DE-AC04-94AL85000.

-
- [1] F. Heslot, N. Fraysse, and A. M. Cazabat, *Nature* **338**, 640 (1989).
 - [2] F. Heslot, A. M. Cazabat, and P. Levinson, *Phys. Rev. Lett.* **62**, 1286 (1989).
 - [3] F. Heslot, A. M. Cazabat, P. Levinson, and N. Fraysse, *Phys. Rev. Lett.* **65**, 599 (1990).
 - [4] H. Xu, D. Shirvanyants, K. Beers, K. Matyjaszewski, M. Rubinstein, and S. S. Sheiko, *Phys. Rev. Lett.* **93**, 206103 (2004).
 - [5] J. A. Nieminen, D. B. Abraham, M. Karttunen, and K. Kaski, *Phys. Rev. Lett.* **69**, 124 (1992).
 - [6] U. D'Ortona, J. De Coninck, J. Koplik, and J. R. Banavar, *Phys. Rev. E* **53**, 562 (1996).
 - [7] S. Bekink, S. Karaborni, G. Verbist, and K. Esselink, *Phys. Rev. Lett.* **76**, 3766 (1996).
 - [8] D. R. Heine, G. S. Grest, and E. B. Webb III, *Phys. Rev. E* **68**, 061603 (2003).
 - [9] D. R. Heine, G. S. Grest, and E. B. Webb III, *Phys. Rev. E* **70**, 011606 (2004).
 - [10] D. R. Heine, G. S. Grest, and E. B. Webb III, *Phys. Rev. Lett.* **95**, 107801 (2005).
 - [11] Y. Xia and G. M. Whitesides, *Annu. Rev. Mater. Res.* **28**, 153 (1998).
 - [12] R. Lipowsky, *Curr. Opin. Colloid Interface Sci.* **6**, 40 (2001).
 - [13] A. A. Darhuber and S. M. Troian, *Ann. Rev. Fluid Mech.* **37**, 425 (2005).
 - [14] H. Gau, S. Herminghaus, P. Lenz, and R. Lipowsky, *Science* **283**, 46 (1999).
 - [15] A. A. Darhuber, S. M. Troian, S. M. Miller, and S. Wagner, *J. Appl. Phys.* **87**, 7768 (2000).
 - [16] M. Brinkmann and R. Lipowsky, *J. Appl. Phys.* **92**, 4296 (2002).
 - [17] J. Lèopoldès, A. Dupuis, D. G. Bucknall, and J. M. Yeomans, *Langmuir* **19**, 9818 (2003).
 - [18] A. Dupuis and J. M. Yeomans, *Langmuir* **21**, 2624 (2005).
 - [19] J. Yaneva, A. Milchev, and K. Binder, *J. Chem. Phys.* **123**, 0 (2005).
 - [20] S. Dietrich, M. N. Popescu, and M. Rauscher, *J. Phys.: Condens. Mater.* **17**, S577 (2005).
 - [21] A. Dupuis, J. Lèopoldès, D. G. Bucknall, and J. M. Yeomans, *Cond-mat/* p. 0507335 (2005).
 - [22] M. Pütz, K. Kremer, and G. S. Grest, *Europhys. Lett.* **49**, 735 (2000).
 - [23] K. Kremer and G. S. Grest, *J. Chem. Phys.* **92**, 5057 (1990).
 - [24] O. M. Braun and M. Peyrard, *Phys. Rev. E* **63**, 046110 (2001).
 - [25] S. Plimpton, *J. Comput. Phys.* **117**, 1 (1995).